Zero Threshold for Water Adsorption on MAPbBr$_3$

*Robin Kerr, Thomas J. Macdonald, Alex J. Tanner, Jiangdong Yu, Julia A. Davies, Helen H. Fielding, and Geoff Thornton**

Hybrid organic–inorganic perovskites (HOIPs) have shown great promise in a wide range of optoelectronic applications. However, this performance is inhibited by the sensitivity of HOIPs to various environmental factors, particularly high levels of relative humidity. This study uses X-ray photoelectron spectroscopy (XPS) to determine that there is essentially no threshold to water adsorption on the in situ cleaved MAPbBr$_3$(001) single crystal surface. Using scanning tunneling microscopy (STM), it shows that the initial surface restructuring upon exposure to water vapor occurs in isolated regions, which grow in area with increasing exposure, providing insight into the initial degradation mechanism of HOIPs. The electronic structure evolution of the surface was also monitored via ultraviolet photoemission spectroscopy (UPS), evidencing an increased bandgap state density following water vapor exposure, which is attributed to surface defect formation due to lattice swelling. This study will help to inform the surface engineering and designs of future perovskite-based optoelectronic devices.

1. Introduction

Hybrid Organic–Inorganic Perovskites (HOIPs) have garnered significant interest worldwide since their use was first reported in a photovoltaic context, as a nanocrystalline sensitizer on TiO$_2$.[1]

R. Kerr, A. J. Tanner, J. Yu, J. A. Davies, H. H. Fielding, G. Thornton
Department of Chemistry
University College London
London WC1H 0AJ, UK
E-mail: g.thornton@ucl.ac.uk
R. Kerr, A. J. Tanner, J. Yu, G. Thornton
London Centre for Nanotechnology
University College London
London WC1H 0AH, UK
T. J. Macdonald
Department of Chemistry & Centre for Processable Electronics
Imperial College London
London W12 0BZ, UK
T. J. Macdonald
School of Engineering & Materials Science
Queen Mary University of London
London E1 4NS, UK

In little over a decade, the power conversion efficiency has reached 25.7% in a single-junction perovskite solar cell (PSC) and 32.5% in a tandem architecture with crystalline silicon,[2] owing in large part to HOIPs' high light absorption coefficients, tunable direct bandgaps, low exciton binding energies, and long carrier diffusion lengths.[3] These efficiencies are comparable to those of conventional solar cells, notably those based on Si, CdTe, and CuIn$_{1-x}$Ga$_x$Se$_2$ (CIGS),[4] while PSCs offer the added benefit of lower manufacturing costs and simpler processing techniques. Beyond applications in solar cells, HOIPs have shown promise in light-emitting diodes,[5] lasers,[6] and photocatalytic systems.[7] A typical PSC device features a polycrystalline thin film, which displays a relatively high density of trap states,[8] suggesting that there is potential for further improvement in device performance through the use of single crystals,[9] with their lower trap densities and higher carrier mobilities.[10]

The impressive properties of HOIPs are fundamentally determined by the lattice structure. The stoichiometry is given by ABX$_3$, where the A site is occupied by an organic cation (typically methylammonium, MA$^+$ or formamidinium, FA$^+$), B a heavy metal cation (Pb^{2+} or Sn^{2+}) and X a halide (I$^-$, Br$^-$, or Cl$^-$). The structure can be considered as two interpenetrating sublattices, with an inorganic sublattice of corner-shared BX$_6^{4-}$ octahedra (overall stoichiometry BX$_3^-$) and an organic sublattice of A$^+$ cations. Charge transport occurs primarily within the inorganic sublattice,[11] while the organic cations serve to modulate the electrostatic landscape experienced by the charge carriers.[12]

Stability against factors such as heat and light remains a major obstacle to the upscaling of PSCs.[13] In addition, HOIPs are notoriously sensitive to moisture,[14] which has a deleterious impact on device performance.[14a,b,d] Encapsulation and additive or interface engineering may offer promising solutions,[15] but the degradation pathways of HOIPs under different environmental conditions must be further understood. This will serve as a basis to develop more stable compositions and device architectures, which will contribute to the goal of achieving a PSC field stability on the scale of 25 years to match the standards of conventional silicon solar cells.[16]

The advent of methods to readily synthesize high-quality, millimeter-scale single crystals provided new prospects for fundamental studies in addition to single crystal-based device engineering. In particular, MAPbBr$_3$ displays superior ease of

**ADVANCED
SCIENCE NEWS**
www.advancedsciencenews.com
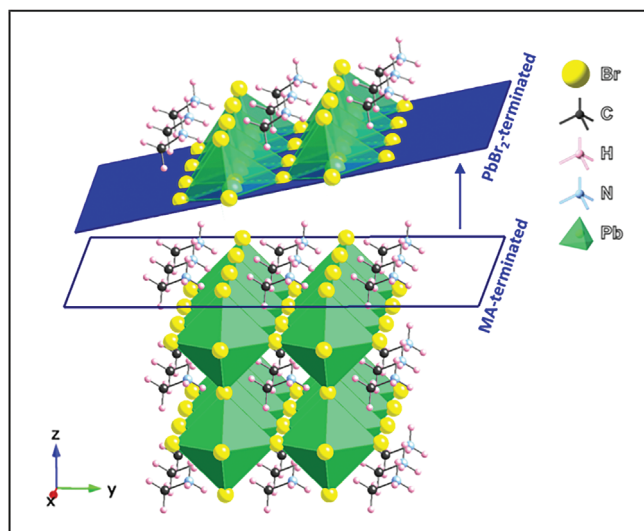
NANO · MICRO
small
www.small-journal.com

Figure 1. Schematic diagram of the cubic MAPbBr$_3$ structure cleaved along the (001) plane. The two surface terminations, the MA-terminated surface and the PbBr$_2$-terminated surface, are labelled. Yellow spheres represent bromine ions, with carbon shown in grey, nitrogen in blue, hydrogen in pink, and lead octahedra shaded green.

Figure 2. XPS (Mg Kα, $h\nu$ = 1253.6 eV) survey scans of a) the in situ cleaved, pristine MAPbBr$_3$ (001) surface and b) the same surface after being exposed to 100 L water vapor. The blue vertical line highlights the small but noticeable O 1s peak at 533.3 eV, which appears by 100 L of water vapor exposure.

synthesis and air-stability to MAPbI$_3$,[10b,c] as well as an intrinsic (001) cleave plane[17] (**Figure 1**), which has led to MAPbBr$_3$ being considered a prototypical HOIP single crystal for surface studies under ultra-high vacuum (UHV) conditions (defined by pressures of 10^{-9} mbar or below). Previous work by Murali et al. on MAPbBr$_3$ single crystals in UHV revealed the surface restructuring in real space following exposure to ambient air. Using scanning tunneling microscopy (STM), the lattice was shown to swell, providing further evidence for a hydrated phase, which was corroborated by X-ray photoelectron spectroscopy (XPS).[14b] Also using XPS, in situ water-dosing experiments on the surface of the same material carried out by Wang et al. found a reaction threshold of 10^8 L (1 Langmuir = 1.33×10^{-6} mbar s), beyond which the crystal began to decompose; at exposures below this threshold there was no chemical reaction.[18] Using atomic force microscopy, Choi et al. imaged clusters of crystalline PbBr$_2$ that formed on the MAPbBr$_3$ surface over a timeframe of several weeks. It was concluded that over this time, CH$_2$NH$_2^+$ would desorb favorably in the presence of hydroxyl radicals and hydroxide ions present in the chamber, leaving a Pb-rich surface.[19] It should be highlighted that the net effect of hydration of the surface on carrier collection in a HOIP-based device is detrimental as a result of interfacial contact resistance.[14b]

Despite surface stability being a significant challenge to the development of HOIP-based devices, experimental investigations of the initial interaction between the HOIP surface and water molecules are lacking. In this work, a systematic study is presented of in situ cleaved MAPbBr$_3$ surface restructuring under low exposures (≤100 L) of water vapor under highly controlled conditions, with the electronic and structural changes monitored using XPS, ultraviolet photoemission spectroscopy (UPS) and STM. The threshold to water adsorption is determined, and nanostructured features are visualized that typify the restructuring of the lattice due to water uptake. These findings reveal cru-
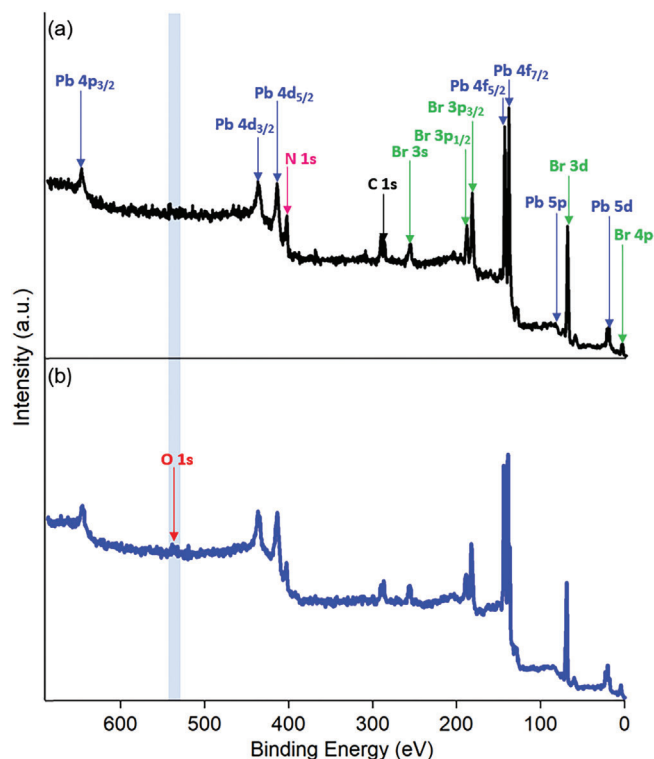
cial information regarding the structure of the HOIP surface after even ultra-low exposures to water vapor. Understanding the initial mechanistic degradation steps will be key to the development of future, more stable PSC devices.

2. Results and Discussion

Figure 2a shows an XPS spectrum of the in situ cleaved MAPbBr$_3$ (001). A MAPbBr$_3$ single crystal exposed to atmosphere possesses a significant oxygen content due to water uptake and other ambient degradation processes (Figure S2, Supporting Information), therefore, the absence of a discernible signal from O 1s confirms the cleanliness of the surface. There was no discernible shift in the core level binding energies of any elements during these experiments at low water vapor exposures, consistent with the conclusion from Wang et al. that there is no chemical reaction between water and MAPbBr$_3$ until much higher exposures of 10^8 L.[18]

Having established the cleanliness of the surface, water vapor was dosed onto the surface in increasing factors of ten from 0.1 to 100 L inclusive. The XPS spectrum following 100 L exposure is shown in Figure 2b, which evidences the formation of an O 1s peak at 533.3 eV. **Figures 3**a–e display how this peak evolves as the water vapor exposure is increased. In Figure 3a the O 1s signal intensity was especially weak. However, a peak could be fitted, the area of which corresponded to ≈0.01 L of water vapor
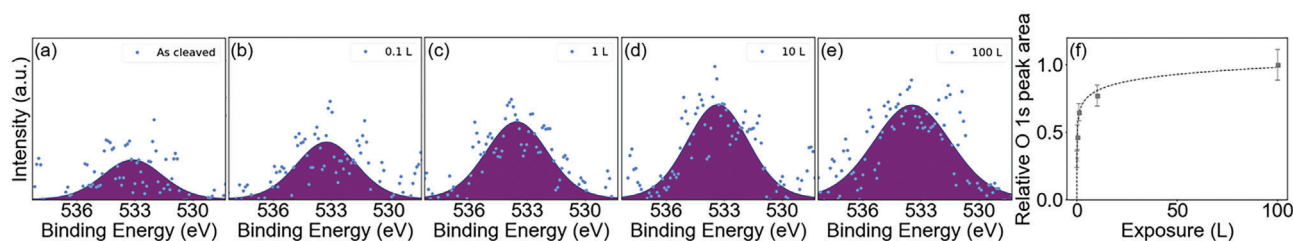
**ADVANCED
SCIENCE NEWS**

www.advancedsciencenews.com

NANO · MICRO

small

www.small-journal.com

Figure 3. Evolution of the O 1s peak where MAPbBr$_3$ (001) has been deliberately exposed to a) 0 L, b) 0.1 L, c) 1 L, d) 10 L, and e) 100 L water vapor in situ via high precision leak valve. f) Scatter plot comparing peak area with exposure. The point corresponding to (a), marked by a cross, was superimposed onto the other four points' best fit curve.

exposure (from Figure 3f), which we assign to residual water in UHV before XPS measurements. The O 1s peak that can be seen to develop in Figures 3a–e at 533.3 eV has been observed as a shoulder on the O 1s peak on an aged MAPbBr$_3$ surface and attributed to molecular water in the literature.[14b,20] The thickness of the water layer following 100 L of water exposure was calculated to be 0.25 MLE (monolayer equivalent, which is the coverage that would be present if the entire adsorbate existed on the surface with exactly one layer), see Section 4. As will be described in the following paragraphs, the coverage was found to be inhomogeneous, so the actual take-up is expected to be higher. Therefore, the value of 0.25 MLE, corresponding to a sticking coefficient of 2.5×10^{-3} at this exposure, is considered a lower limit estimate. Taking one monolayer as one water molecule per unit cell,[14f] the density of water molecules following 100 L of water vapor exposure therefore approximate to 7.1×10^{13} cm^{-2}. We note that MAPbI$_3$ is known to undergo a color change upon hydration to MAPbI$_3$·H$_2$O;[14d] such a color change was not observed here. This likely evidences an early stage in the stepwise perovskite hydration (to, for instance, 4MAPbBr$_3$·H$_2$O).[21] Figure 3f displays a rapid take-up before plateauing, demonstrating that water adsorption occurs with no threshold. Indeed, the initial sticking coefficient, where the take-up is linear, is unity within the errors. Our XPS on the aged surface and UPS He-II measurements on the in situ cleaved surface (Figures S2 and S3, Supporting Information) were consistent with molecular water adsorption, while He-I measurements of the valence band region (Figure S4, Supporting Information) showed no evidence of disruption to the lattice.

The surface morphology of MAPbBr$_3$(001) was probed by STM following the same water vapor exposures as in Figure 3 (increasing from 0.1 L to 100 L in factors of 10). As expected for a crystalline material, the pristine surface displays layer-after-layer stacking, shown in **Figure 4**a, with a step height corresponding to the unit cell length in the [001] direction of 5.92 Å (Figure S6, Supporting Information). The surface termination could not be determined based on this, but a mix between MA- and PbBr$_2$-terminated surfaces is expected based on atomic force microscopy (AFM) measurements by Choi et al.[22] The surface topography is similar to that reported previously.[14b] Figure S7 (Supporting Information) shows a further example of the terraced structure as first reported by Ohmann et al.[23]

Increasing exposures to water vapor can be seen to cause the formation of isolated regions of restructuring on the surface, comprising individual protrusions; see Figures 4c–e. As the exposure increased, the protrusions became more numerous, and the

restructured regions increased in surface area, eventually linking together. It is expected that this clustering is due to hydrogen bonding between water molecules.[14e] By 10 L of water vapor exposure (Figure 4d), a significant area of the image can clearly be seen to have been reconstructed. By 100 L (Figure 4e), the surface looks similar to an aged MAPbBr$_3$ surface, i.e., one that has been exposed to ambient conditions; similar features are reported here to those observed on the aged surface, including so-called disunified 1D chains and ringlike protrusions.[14b] Recent AFM and XPS studies on FAPbI$_3$ thin films at elevated humidity have also shown a similar restructuring on the (100) facets.[24] We note that the relative amplitude of each image decreases with increasing water vapor exposure, consistent with relaxation of the as-cleaved surface by restructuring.

The hydrate ultimately formed by water exposure has been suggested as a model system for epitaxial growth of perovskite hydrate on a single crystalline surface,[14b] where the hydrate experiences tensile strain induced by the lattice mismatch with the pristine surface. The strain is released via formation of nanostructures. Such structures are clearly visible following exposure to 100 L water vapor. Furthermore, the nucleation-based growth of the restructured regions on the single crystalline surface is consistent with the Volmer-Weber model. This heterogeneous island growth could be associated with the local orientation of methylammonium atoms close to the surface; using density functional theory, Koocher et al. found that the polarity determined whether molecules were adsorbed on the perovskite surface or were trapped in a top layer interstitial space.[25] This is also consistent with the finite temperature molecular dynamics performed by Caddeo et al., which found water vapor infiltration to be possible, though less energetically favorable than adsorption.[26] Figure 4f depicts the corresponding line profiles, where the red, green, and black lines indicate the profile of the ringlike protrusion and the length and width of the disunified 1D chain, respectively.

Having established that by 100 L exposure, the MAPbBr$_3$ surface shows similar features to that seen for its aged counterpart, we present in **Figure 5** laser UPS ($h\nu$ = 6.2 eV) spectra of the bandgap states. It is known that the clean MAPbBr$_3$ surface (black line) possesses a density of bandgap states that can be probed by photoemission spectroscopy.[27] The inset shows the bandgap region of the spectra following removal of the secondary electron background (which, at this photon energy, is enhanced by excitation from the valence band maximum[27,28]) with a Tougaard function. The spectrum from the surface exposed to 100 L water vapor (blue line) shows a broad increase in the
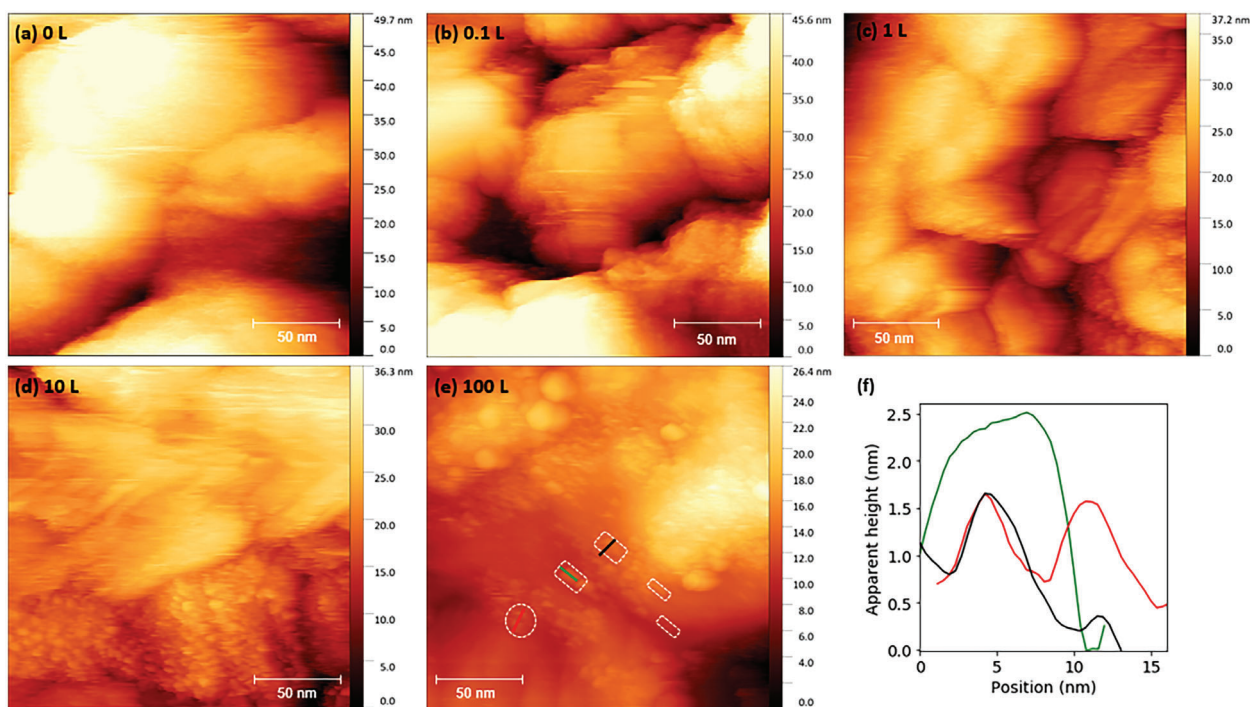
Figure 4. Real-space imaging of an in situ cleaved MAPbBr$_3$(001) surface by STM after deliberate exposure to a) 0 L, b) 0.1 L, c) 1 L, d) 10 L and e) 100 L water vapor, recorded with scanning parameters of V_b = 2.5 V and I_t = 0.1 nA. Ringlike protrusions are marked by circles and disunified 1D chains by rectangles, indicating the intercalation of molecular water. f) Line profiles corresponding to (e), where the length and diameter of the 1D chains are represented in green and black, respectively, and the line profile on a ringlike protrusion is shown in red.
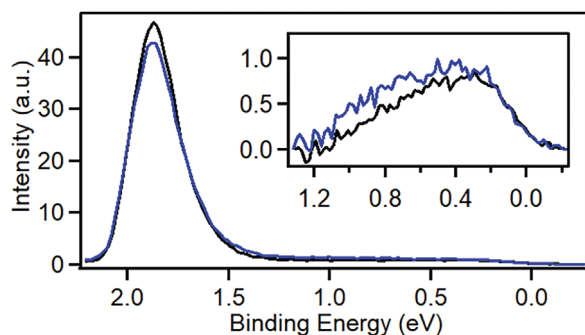

Figure 5. UPS ($h\nu$ = 6.2 eV) spectra from freshly cleaved (black line) MAPbBr$_3$(001), and the same surface following exposure to 100 L water vapor (blue line). The inset compares the spectra following removal of a Tougaard background, illustrating a water-induced increase in the density of gap states.

density of bandgap states centered about 0.7 eV below the Fermi level. These states have been associated with structural defects, likely undercoordinated Pb sites.[29] Their increase with water adsorption suggests that strain associated with surface restructuring is released through the formation of more surface defects. It is possible that the physical cleavage of the surface induces tensile strain a factor that has been shown to decrease the stability of HOIP thin films to humidity.[30] Lattice mismatch between the restructured perovskite and pristine substrate is likely to induce further strain (as has been shown between HOIP thin films and substrates[31]), which could accelerate water uptake. No change

in the bandgap state binding energy can be observed, suggesting that the electronic environment of the defect has not changed, but that the defect density is being increased. The increase is corroborated by the UPS He-I spectra in Figure S4 (Supporting Information). It is likely that this increase in occupied states near the Fermi level contributes to the decrease in electrical resistance previously observed on HOIPs in the presence of moisture.[32] The UPS measurements were performed on a freshly cleaved crystal, as it is known that X-ray irradiation induces Pb^0 defects on MAPbBr$_3$.[18,33]

These conclusions have implications from a device perspective: PSC devices typically require encapsulation in order to increase their photostability.[34] Furthermore, common hole-transporting layers used in PSCs, such as 2,2′,7,7′-tetrakis(N,N-di-p-methoxyphenylamine)-9-9′-spirobifluorene (Spiro-OMeTAD) are permeable to water and constitute a poor moisture barrier.[35] Therefore, under ambient conditions, the active layer of a PSC is likely to be exposed to water vapor to some degree. Whether a HOIP single crystal is the active layer of a device or is considered a model for the fundamental understanding of its polycrystalline counterparts, our findings effectively demonstrate the importance of the interaction between water and HOIP surfaces at ultra-low water vapor pressure.

3. Conclusion

In summary, the in situ cleaved surface of the prototypical single crystal perovskite MAPbBr$_3$ has been exposed to water vapor under UHV conditions up to 100 L, demonstrating a

**ADVANCED
SCIENCE NEWS**

www.advancedsciencenews.com

NANO · MICRO
small

www.small-journal.com

susceptibility to water adsorption. Insight was provided into the surface restructuring mechanism at these low exposures: XPS revealed the development of the O 1s peak as water vapor exposure was increased. Using STM, the nanoscale nucleation-based growth of reconstructed facets has been observed directly: restructuring was shown to occur in isolated regions at first, in line with previously reported first principles calculations,[14e] which grew and connected with increasing exposure. By 100 L of water vapor exposure, the surface closely resembled one that had been aged in ambient conditions. Nanostructured features, so-called ringlike protrusions and disunified 1D chains, were identified and confirmed by their line profiles, consistent with the structures previously reported on the aged surface.[14b] UPS measurements provided evidence that the strain induced by the surface restructuring was released via surface defect formation. This work will help to inform future surface engineering and design of perovskite-based optoelectronic devices. Future work may investigate the surface interaction of water vapor with additional single crystal HOIP variants relevant to current research such as $FAPbI_3$ and $CsFAMAPbI_3$.

4. Experimental Section

Chemicals and Reagents: $PbBr_2$ ($\geq$98%) and *N,N*-dimethylformamide (anhydrous, $\geq$99.8%) procured from Sigma–Aldrich and CH_3NH_3Br (>99.99%) procured from *GreatCell Solar* were used for crystal synthesis.

MAPbBr$_3$ Single Crystal Synthesis: $MAPbBr_3$ single crystals were synthesized by the inverse temperature crystallization method.[10b] A 1 mol L^{-1} solution of $PbBr_2$ (Sigma–Aldrich) and CH_3NH_3Br (*GreatCell Solar*) was dissolved in 2 mL anhydrous *N,N*-dimethylformamide (Sigma–Aldrich) in a small vial at room temperature. The vial was placed in an oil bath at 60 °C that was slowly ramped to 80 °C and held for three hours, producing crystals measuring $3 \times 3 \times 2$ mm^3.

Measurement and Characterization: The phase purity and single crystalline nature of the samples were confirmed using powder and single crystal X-ray diffraction (PXRD and SCXRD), respectively. See Figures S6 and S9, and Table S1 (Supporting Information) for unit cell height measured by STM, PXRD diffractogram and SCXRD data, respectively, which were consistent with the literature and reflect the cubic phase of MAPbBr3.[10b,c,19,36]

XPS (*XR3HP, VG Microtech*), He-I and He-II UPS (*VG Microtech*) and laser UPS experiments were performed in one UHV system, with a separate system employed for STM measurements. The two systems had base pressures of $\approx 1 \times 10^{-10}$ mbar, with the partial pressure of residual water $\approx 2 \times 10^{-11}$ mbar, measured by a residual gas analyzer (*Hiden Analytical, HAL 101*). The X-ray light source provided Mg Kα photons ($h\nu = 1253.6$ eV). The photoelectrons were recorded with a hemispherical electron kinetic energy analyzer (*VG Scienta R3000*) normal to the sample surface. The spectra were calibrated to Pb^0 $4f_{7/2}$ (136.8 eV).[37] A Savitzky-Golay function was applied to the water-dosed core level spectra while all fitting was carried out with a LA(1.53,243) (Voigt) fitting function using CasaXPS software. A Shirley background was subtracted to obtain the best fits shown. For He-I, He-II and laser UPS, photoemission from the Ta sample holder was used to determine the position of E_F. 6.2 eV photons for laser UPS were generated by a fourth harmonic generation system pumped by a *Coherent Legend* regenerative amplifier operating at 1 kHz, seeded by a Ti:sapphire oscillator (*Coherent Micra*). The sample was biased by −3.0 V. The laser power was reduced to ≈ 1 μW using a neutral density filter to minimize space charge effects and any laser-induced degradation. In order to check for laser- or UHV-induced defect formation, we performed two tests. First, the laser UPS spectra showed no variation during measurements, even after 20 min of irradiation. Second, on a different, freshly

cleaved sample, two spectra were taken two hours apart, which were identical, ruling out UHV conditions alone as a source of defect formation.

An Omicron AFM/STM operated in constant current mode was used for the STM measurements. Electrochemically etched tungsten tips were used, degassed in UHV and conditioned under voltage pulses of up to +10 V to achieve an atomic-scale 1×1 termination of a clean TiO_2 rutile(110) single crystal. The TiO_2 sample was prepared according to literature methods.[38] To our knowledge, the (001) surface of the $MAPbBr_3$ single crystal had not been imaged at the atomic scale using room temperature STM (Murali et al. assigned their atomic imaging of the $MAPbBr_3$ lattice to the (110) plane[14b]). The reason why atomic resolution on the (001) plane was not possible here or in previous work at room temperature is not clear. One possibility is that it stems from interaction between the tip and the weakly bound organic cations.[39] All STM images were processed using the open-source software Gwyddion.

Each experiment was performed on a freshly cleaved $MAPbBr_3$ crystal at room temperature. For in situ cleaving, the crystal was mounted to a tantalum sample holder using conductive silver epoxy (*EpoTek EJ2189*). A tungsten rod was attached to the crystal using Torr seal (*Varian*). The rod, or cleave post, was removed with a wobble stick in a load-lock vacuum chamber (10^{-7} mbar) and the sample was immediately transferred into UHV (10^{-10} mbar). In this way, a pristine, mirrored $MAPbBr_3$ (001) single crystal surface was achieved. The cleanliness of the surface cleaved by this method was verified using XPS as detailed in Section 2.

Water adsorption on the in situ cleaved $MAPbBr_3$ (001) surface was achieved via gas phase dosing under UHV conditions from an ultrapure liquid sample. Water samples were further cleaned via freeze-pump-thaw cycles to remove any dissolved contaminant gases. The purity of the water vapor was monitored using a residual gas analyzer (*Hiden Analytical, HAL 101*).

It is known that upon X-ray irradiation in vacuum, the HOIP surface gradually degrades to metallic lead,[18,33,40] saturating at around 10% of the initial Pb 4f intensity.[18] It was for this reason that the bandgap state measured by UPS (rather than Pb 4f shoulders measured by XPS) was used to gauge water-induced defect formation. Furthermore, in order to estimate the thickness of the water layer on $MAPbBr_3$ (001), the Pb 4f signal following water exposure was compared to the signal following the same X-ray dose, but without water, according to Equation (1),

$$\frac{I_{H_2O,X-ray}}{I_{X-ray}} = \exp\left(-\frac{d_W^L}{\lambda_W^L \cos \theta}\right), \tag{1}$$

where $I_{H_2O,X-ray}$ and I_{X-ray} are the Pb 4f signal intensities for samples with and without water dosing, respectively, λ_W^L is the inelastic mean free path for an electron in liquid water (calculated using the NIST Inelastic Mean Free Path Database (version 1.2), for a photon energy of 1253.6 eV), θ the angle between the surface normal and the analyzer axis (0°), and d_W^L the thickness of the surface water layer. Substituting the appropriate constants following a water exposure of 100 L yields a water layer thickness of 0.063 nm. If the thickness of one monolayer (ML) of water is taken to be 0.25 nm, the average water layer thickness was therefore 0.25 MLE.

Supporting Information

Supporting Information is available from the Wiley Online Library or from the author.

Acknowledgements

Conflict of Interest

The authors declare no conflict of interest.

Data Availability Statement

The data that support the findings of this study are available from the corresponding author upon reasonable request.

Keywords

crystal structures, crystals, perovskites, scanning tunneling microscopy, surface science

[1] A. Kojima, K. Teshima, Y. Shirai, T. Miyasaka, *J. Am. Chem. Soc.* **2009**, *131*, 6050.

[2] NREL, Best Research Cell Efficiencies, https://www.nrel.gov/pv/cell-efficiency.html (accessed: April 2023).

[3] a) K. Zheng, Q. Zhu, M. Abdellah, M. E. Messing, W. Zhang, A. Generalov, Y. Niu, L. Ribaud, S. E. Canton, T. Pullerits, *J. Phys. Chem. Lett.* **2015**, *6*, 2969; b) J. H. Noh, S. H. Im, J. H. Heo, T. N. Mandal, S. I. Seok, *Nano Lett.* **2013**, *13*, 1764; c) H.-S. Kim, C.-R. Lee, J.-H. Im, K.-B. Lee, T. Moehl, A. Marchioro, S.-J. Moon, R. Humphry-Bar, J.-H. Yum, J. E. Moser, M. Grätzel, N.-G. Park, *Sci. Rep.* **2012**, *2*, 591; d) S. Chen, G. Shi, *Adv. Mater.* **2017**, *9*, 1605448.

[4] M. I. H. Ansari, A. Qurashi, M. K. Nazeeruddin, *J. Photochem. Photobiol. C Photochem. Rev.* **2018**, *35*, 1.

[5] X. Zhang, W. Yin, W. Zheng, A. L. Rogach, *ACS Energy Lett.* **2020**, *5*, 2927.

[6] Y. Jia, R. A. Kerner, A. J. Grede, A. N. Brigeman, B. P. Rand, N. C. Giebink, *Nano Lett.* **2016**, *16*, 4624.

[7] a) H. Huang, B. Pradhan, J. Hofkens, M. B. J. Roeffaers, J. A. Steele, *ACS Energy Lett.* **2020**, *5*, 1107; b) S. Park, W. J. Chang, C. W. Lee, S. Park, H. Y. Ahn, K. T. Nam, *Nat. Energy* **2016**, *2*, 1.

[8] D. Luo, R. Su, W. Zhang, Q. Gong, R. Zhu, *Nat. Rev. Mater.* **2020**, *5*, 44.

[9] a) A. Capitaine, B. Sciacca, *Adv. Mater.* **2021**, *33*, 2102588; b) B. Murali, E. Yengel, C. Yang, W. Peng, E. Alarousu, O. M. Bakr, O. F. Mohammed, *ACS Energy Lett.* **2017**, *2*, 846; c) J. Li, Y. Gu, Z. Han, J. Liu, Y. Zou, X. Xu, *J. Phys. Chem. Lett.* **2022**, *13*, 274; d) B. Turedi, V. Yeddu, X. Zheng, D. Y. Kim, O. M. Bakr, M. I. Saidaminov, *ACS Energy Lett.* **2021**, *6*, 631; e) Z. Chen, B. Turedi, A. Y. Alsalloum, C. Yang, X. Zheng, I. Gereige, A. AlSaggaf, O. F. Mohammed, O. M. Bakr, *ACS Energy Lett.* **2019**, *4*, 1258; f) A. Y. Alsalloum, B. Turedi, K. Almasabi,

X. Zheng, R. Naphade, S. D. Stranks, O. F. Mohammed, O. M. Bakr, *Energy Environ. Sci.* **2021**, *14*, 2263; g) A. Y. Alsalloum, B. Turedi, X. Zheng, S. Mitra, A. A. Zhumekenov, K. Lee, P. Maity, I. Gereige, A. AlSaggaf, I. S. Roqan, O. F. Mohammed, O. M. Bakr, *ACS Energy Lett.* **2020**, *5*, 657.

[10] a) J. S. Manser, J. A. Christians, P. V. Kamat, *Chem. Rev.* **2016**, *116*, 12956; b) M. I. Saidaminov, A. L. Abdelhady, B. Murali, E. Alarousu, V. M. Burlakov, W. Peng, I. Dursun, L. Wang, Y. He, G. Maculan, A. Goriely, T. Wu, O. F. Mohammed, O. M. Bakr, *Nat. Commun.* **2015**, *6*, 1; c) D. Shi, V. Adinolfi, R. Comin, M. Yuan, E. Alarousu, A. Buin, Y. Chen, S. Hoogland, A. Rothenberger, K. Katsiev, Y. Losovyj, X. Zhang, P. A. Dowben, O. F. Mohammed, E. H. Sargent, O. M. Bakr, *Science* **2015**, *347*, 519; d) W. Peng, X. Miao, V. Adinolfi, E. Alarousu, O. El Tall, A.-H. Emwas, C. Zhao, G. Walters, J. Liu, O. Ouellette, J. Pan, B. Murali, E. H. Sargent, O. F. Mohammed, O. M. Bakr, *Angew. Chem., Int. Ed.* **2016**, *55*, 10686; e) A. A. Zhumekenov, M. I. Saidaminov, M. A. Haque, E. Alarousu, S. P. Sarmah, B. Murali, I. Dursun, X.-H. Miao, A. L. Abdelhady, T. Wu, O. F. Mohammed, O. M. Bakr, *ACS Energy Lett.* **2016**, *1*, 32.

[11] M. H. Du, *J. Mater. Chem. A.* **2014**, *2*, 9091.

[12] H. Zhu, K. Miyata, Y. Fu, J. Wang, P. Joshi, D. Niesner, K. W. Williams, S. Jin, X.-Y. Zhu, *Science* **2016**, *353*, 1409.

[13] a) J.-Y. Ma, J. Ding, H.-J. Yan, D. Wang, J.-S. Hu, *ACS Appl. Mater. Interfaces* **2019**, *11*, 21627; b) R. K. Misra, S. Aharon, B. Li, D. Mogilyansky, I. Visoly-Fisher, L. Etgar, E. A. Katz, *J. Phys. Chem. Lett.* **2014**, *6*, 326; c) D. Bryant, N. Aristidou, S. Pont, I. Sanchez-Molina, T. Chotchuangchutchaval, S. Wheeler, J. R. Durrant, S. A. Haque, *Energy Environ. Sci.* **2016**, *9*, 1655; d) Y. Han, S. Meyer, Y. Dkhissi, K. Weber, J. M. Pringle, U. Bach, L. Spiccia, Y.-B. Cheng, *J. Mater. Chem. A.* **2015**, *3*, 8139.

[14] a) J. A. Christians, P. A. M. Herrera, P. V. Kamat, *J. Am. Chem. Soc.* **2015**, *137*, 1530; b) B. Murali, S. Dey, A. L. Abdelhady, W. Peng, E. Alarousu, A. R. Kirmani, N. Cho, S. P. Sarmah, M. R. Parida, M. I. Saidaminov, A. A. Zhumekenov, J. Sun, M. S. Alias, E. Yengel, B. S. Ooi, A. Amassian, O. M. Bakr, O. F. Mohammed, *ACS Energy Lett.* **2016**, *1*, 1119; c) M. Akhavan Kazemi, P. Raval, K. Cherednichekno, J.-N. Chotard, A. Krishna, A. Demortiere, G. N. M. Reddy, F. Sauvage, *Small Methods* **2021**, *5*, 2000834; d) A. M. A. Leguy, Y. Hu, M. Campoy-Quiles, M. I. Alonso, O. J. Weber, P. Azarhoosh, M. van Schilfgaarde, M. T. Weller, T. Bein, J. Nelson, P. Docampo, P. R. F. Barnes, *Chem. Mater.* **2015**, *27*, 3397; e) C.-J. Tong, W. Geng, Z.-K. Tang, C.-Y. Yam, X.-L. Fan, J. Liu, W.-M. Lau, L.-M. Liu, *J. Phys. Chem. Lett.* **2015**, *6*, 3289; f) S. Cheng, H. Zhong, *J. Phys. Chem. Lett.* **2022**, *13*, 2281; g) J.-Y. Ma, H.-J. Yan, M.-H. Li, J.-K. Sun, Y.-X. Chen, D. Wan, J.-S. Hu, *Nanoscale* **2020**, *12*, 7759.

[15] a) H. Tsai, W. Nie, J.-C. Blancon, C. C. Stoumpos, R. Asadpour, B. Harutyunyan, A. J. Neukirch, R. Verduzco, J. J. Crochet, S. Tretiak, L. Pedesseau, J. Even, M. A. Alam, G. Gupta, J. Lou, P. M. Ajayan, M. J. Bedzyk, M. G. Kanatzidis, A. D. Mohite, *Nature* **2016**, *536*, 312; b) C.-T. Lin, W. Xu, T. J. Macdonald, J. Ngiam, J.-H. Kim, T. Du, S. Xu, P. S. Tuladhar, H. Kang, K. Lee, J. R. Durrant, M. A. McLachlan, *ACS Appl. Mater. Interfaces* **2021**, *13*, 43505; c) T. J. Macdonald, A. J. Clancy, W. Xu, Z. Jiang, C.-T. Lin, L. Mohan, T. Du, D. D. Tune, L. Lanzetta, G. Min, T. Webb, A. Ashoka, R. Pandya, V. Tileli, M. A. McLachlan, J. R. Durrant, S. A. Haque, C. A. Howard, *J. Am. Chem. Soc.* **2021**, *143*, 21549.

[16] R. Roesch, T. Faber, E. von Hauff, T. M. Brown, M. Lira-Cantu, H. Hoppe, *Adv. Energy Mater.* **2015**, *5*, 1501407.

[17] H.-C. Hsu, B.-C. Huang, S.-C. Chin, C.-R. Hsing, D.-L. Nguyen, M. Schnedler, R. Sankar, R. E. Dunin-Borkowski, C. M. Wei, C.-W. Chen, P. Ebert, Y.-P. Chiu, *ACS Nano* **2019**, *13*, 4402.

[18] C. Wang, B. R. Ecker, H. Wei, J. Huang, Y. Gao, *J. Phys. Chem. C* **2018**, *122*, 3513.

[19] J. I. J. Choi, M. E. Khan, Z. Hawash, K. J. Kim, H. Lee, L. K. Ono, Y. Qi, Y.-H. Kim, J. Y. Park, *J. Mater. Chem. A.* **2019**, *7*, 20760.

[20] D. Halwidl, B. Stoger, W. Mayr-Schmolzer, J. Pavelec, D. Fobes, J. Peng, Z. Mao, G. S. Parkinson, M. Schmid, F. Mittendorfer, J. Redinger, U. Diebold, *Nat. Mater.* **2015**, *15*, 450.

[21] G. Grancini, V. D'Innocenzo, E. R. Dohner, N. Martino, A. R. Srimath Kandada, E. Mosconi, F. De Angelis, H. I. Karunadasa, E. T. Hoke, A. Petrozza, *Chem. Sci.* **2015**, *6*, 7305.

[22] J. I. J. Choi, M. E. Khan, Z. Hawash, H. Lee, L. K. Ono, Y. Qi, Y.-H. Kim, J. Y. Park, *J. Phys. Chem. C* **2019**, *124*, 1484.

[23] R. Ohmann, L. K. Ono, H.-S. Kim, H. Lin, M. V. Lee, Y. Li, N.-G. Park, Y. Qi, *J. Am. Chem. Soc.* **2015**, *137*, 16049.

[24] C. Ma, F. T. Eickemeyer, S.-H. Lee, D.-H. Kang, S. J. Kwon, M. Grätzel, N.-G. Park, *Science* **2023**, *379*, 173.

[25] N. Z. Koocher, D. Saldana-Greco, F. Wang, S. Liu, A. M. Rappe, *J. Phys. Chem. Lett.* **2015**, *6*, 4371.

[26] C. Caddeo, M. I. Saba, S. Meloni, A. Filipetti, A. Mattoni, *ACS Nano* **2017**, *11*, 9183.

[27] I. Levine, K. Shimizu, A. Lomuscio, M. Kulbak, C. Rehermann, A. Zohar, M. Abdi-Jalebi, B. Zhao, S. Siebentritt, F. Zu, N. Koch, A. Kahn, G. Hodes, R. H. Friend, H. Ishii, D. Cahen, *J. Phys. Chem. C.* **2021**, *125*, 5217.

[28] J. Endres, D. A. Egger, M. Kulbak, R. A. Kerner, L. Zhao, S. H. Silver, G. Hodes, B. P. Rand, D. Cahen, L. Kronik, A. Kahn, *J. Phys. Chem. Lett.* **2016**, *7*, 2722.

[29] a) S. Yang, S. Chen, E. Mosconi, Y. Fang, X. Xiao, C. Wang, Y. Zhou, Z. Yu, J. Zhao, Y. Gao, F. De Angelis, J. Huang, *Science* **2019**, *365*, 473; b) Z. Ni, C. Bao, Y. Liu, Q. Jiang, W.-Q. Wu, S. Chen, X. Dai, B. Chen, B. Hartweg, Z. Yu, Z. Holman, J. Huang, *Science* **2020**, *367*, 1352; c) N. K. Noel, A. Abate, S. D. Stranks, E. S. Parrott, V. M. Burlakov, A.

[30] Goriely, H. J. Snaith, *ACS Nano* **2014**, *8*, 9815; d) M. L. Agiorgousis, Y.-Y. Sun, H. Zeng, S. Zhang, *J. Am. Chem. Soc.* **2014**, *136*, 14570.

[30] a) J. Wu, S.-C. Liu, Z. Li, S. Wang, D.-J. Xue, Y. Lin, J-. S. Hu, *Natl. Sci. Rev.* **2021**, *8*, nwab047; b) N. Rolston, K. A. Bush, A. D. Printz, A. Gold-Parker, Y. Ding, M. F. Toney, M. D. McGehee, R. H. Dauskardt, *Adv. Energy Mater.* **2018**, *8*, 1802139.

[31] a) Y. Chen, Y. Lei, Y. Li, Y. Yu, J. Cai, M.-H. Chiu, R. Rao, Y. Gu, C. Wang, W. Choi, H. Hu, C. Wang, Y. Li, J. Song, J. Zhang, B. Qi, M. Lin, Z. Zhang, A. E. Islam, B. Maruyama, S. Dayeh, L.-J. Li, K. Yang, Y.-H. Lo, S. Xu, *Nature* **2020**, *577*, 209; b) Y. Rakita, S. R. Cohen, N. K. Kedem, G. Hodes, D. Cahen, *MRS Commun.* **2015**, *5*, 623.

[32] L. Hu, G. Shao, T. Jiang, D. Li, X. Lv, H. Wang, X. Liu, H. Song, J. Tang, H. Liu, *ACS Appl. Mater. Interfaces* **2015**, *7*, 25113.

[33] J. Hieulle, X. Wang, C. Stecker, D.-Y. Son, L. Qiu, R. Ohmann, L. K. Ono, A. Mugarza, Y. Yan, Y. Qi, *J. Am. Chem. Soc.* **2019**, *141*, 3515.

[34] L. Shi, M. P. Bucknall, T. L. Young, M. Zhang, L. Hu, J. Bing, D. S. Lee, J. Kim, T. Wu, N. Takamure, D. R. McKenzie, S. Huang, M. A. Green, A. W. Y. Ho-Baillie, *Science* **2020**, *368*, eaba2412.

[35] a) S. N. Habisreutinger, T. Leijtens, G. E. Eperon, S. D. Stranks, R. J. Nicholas, H. J. Snaith, *Nano Lett.* **2014**, *14*, 5561; b) F. M. Rombach, S. A. Haque, T. J. Macdonald, *Energy Environ. Sci.* **2021**, *14*, 5161.

[36] K. Miyata, D. Meggiolaro, M. T. Trinh, P. P. Joshi, E. Mosconi, S. C. Jones, F. De Angelis, X.-Y. Zhu, *Sci. Adv.* **2017**, *3*, e1701217.

[37] J. C.-R. Ke, A. S. Walton, D. J. Lewis, A. Tedstone, P. O'Brien, A. G. Thomas, W. R. Flavell, *Chem. Commun.* **2017**, *53*, 5231.

[38] O. B. J. Williams, K. Katsiev, B. Baek, G. Harrison, G. Thornton, H. Idriss, *J. Am. Chem. Soc.* **2022**, *144*, 1034.

[39] S. Dey, personal communication.

[40] G. Sadhougi, D. E. Starr, E. Handick, S. D. Stranks, M. Gorgoi, R. G. Wilks, M. Bär, H. J. Snaith, *ACS Appl. Mater. Interfaces* **2015**, *7*, 13440.